

Magnetic excitations in ferro-pnictide materials controlled by a quantum critical point into hidden order

J.P. Rodriguez¹

¹*Department of Physics and Astronomy,
California State University, Los Angeles, California 90032*

(Dated: February 22, 2024)

Abstract

The two-orbital J_1 - J_2 model that describes a square lattice of frustrated spin-1 iron atoms is analyzed within the linear spin-wave approximation and by exact diagonalization over a 4×4 cluster. A quantum critical point (QCP) is identified that separates hidden magnetic order at weak Hund's rule coupling from a commensurate spin density wave (cSDW) at strong Hund's rule coupling. Although the moment for cSDW order is small at the QCP, the critical linear spin-wave spectrum shows strong low-energy excitations centered at the wavenumbers that correspond to cSDW order. These disperse anisotropically. A fit to the magnetic excitation spectrum of ferro-pnictide materials obtained recently by inelastic neutron scattering measurements notably accounts for the absence of softening at the wavenumber that corresponds to Néel order.

I. INTRODUCTION

The discovery of ferro-pnictide superconductors has set a new and unforeseen direction in the search for high-temperature superconductivity.¹ A common structural feature of these materials are square lattices of iron atoms that are stacked up on top of each other.² Density functional theory (DFT) calculations find that the iron 3d orbitals contribute most of the electronic spectral weight near the Fermi surface.^{3,4} This implies that the iron 3d electrons surprisingly play an active role in the superconductivity. In contrast, DFT calculations also predict that the iron moments order antiferromagnetically along the a and along the c axes of the iron lattice at low temperature in the undoped parent compounds,⁵ with an ordered moment of approximately 2 Bohr magnetons (μ_B).⁶ Elastic neutron diffraction studies have confirmed the prediction of long-range commensurate spin-density wave (cSDW) order, but they find a much lower ordered moment that can be a small fraction of the Bohr magneton ($0.36 \mu_B$) in some cases.² It was suggested early on that Heisenberg exchange between both nearest-neighbor (J_1) and next-nearest neighbor (J_2) spins on a square lattice of iron atoms could account for the low ordered moment that is observed because of magnetic frustration.⁷ Recent calculations based on the linear spin-wave approximation⁸ indicate that this effect requires fine tuning however,⁹ and that it occurs only very close to the point of maximum frustration, $J_2 = 0.5 J_1$. A possibly more viable explanation is that the low ordered cSDW moment commonly observed in ferro-pnictide parent compounds is due to proximity to hidden magnetic order among particular iron 3d orbitals such that the magnetic moments cancel out per iron atom. The author and Rezayi have shown that such violations of Hund's rule can occur in multi-orbital Heisenberg models with off-diagonal frustration.¹⁰

Spin-wave excitations of the cSDW groundstate have also been detected in parent compounds to ferro-pnictide superconductors at low temperature by inelastic neutron scattering.^{11,12} Contrary to the prediction of the conventional J_1 - J_2 model over the square lattice however,¹³ the measured spin-wave spectrum fails to soften at the wave number associated with Néel order, $(\pi/a, \pi/a)$. Here a denotes the square lattice constant. It shows a local maximum there instead.¹⁴ Fits to the measured spin-wave dispersion invoke unphysically large anisotropy in the Heisenberg spin exchange across nearest-neighbor links on the square lattice of iron atoms in order to account for the dispersion at the Brillouin zone boundary. More recently, low-energy magnetic excitations centered at the cSDW wave num-

bers have been detected in a ferro-pnictide *superconductor*.¹⁵ These disperse up in energy in an anisotropic fashion that is consistent with the presence of some degree of cSDW order.

In this paper, we continue to explore the hidden magnetic order that is predicted to exist in multi-orbital Heisenberg models over the square lattice when the diagonal and the off-diagonal exchange coupling constants are sufficiently different.¹⁰ Two spin-1/2 orbitals per iron atom are assumed, which implies spin-1 iron moments if Hund’s rule is obeyed. A quantum critical point¹⁶ is identified within the linear spin-wave approximation that separates hidden ferromagnetic or hidden Néel order at weak Hund’s rule coupling from a cSDW at strong Hund’s rule coupling. Numerical exact diagonalizations of the two-orbital Heisenberg model over a 4×4 lattice indicate that the moment associated with cSDW order decays strongly as it enters hidden magnetic order through the putative quantum critical point. The linear spin-wave approximation, on the other hand, finds observable low-energy spin-wave excitations at the quantum critical point that disperse linearly from the cSDW wave numbers in an anisotropic fashion. A spin gap begins to grow there upon entering hidden magnetic order. Observable low-energy spin-wave excitations due to hidden order that are centered at zero momentum are also predicted by the linear spin-wave approximation, but these have very small spectral weight. Fits of the spin-wave spectrum observed by inelastic neutron scattering in ferro-pnictide materials^{14,15} to the critical linear spin-wave spectrum are achieved. They notably account for the dispersion of the low-energy spinwaves centered at the cSDW wave numbers and for the local maximum that exists at the wavenumber associated with Néel order. A critical Hund’s rule coupling of order 100 meV is extracted from these fits. Below we discuss useful theoretical aspects of the Heisenberg model for ferro-pnictide materials⁷ before we go on to analyze it.

II. MULTI-ORBITAL HEISENBERG MODEL

Recent low-temperature measurements of the optical conductivity in the cSDW phase of parent compounds to ferro-pnictide high- T_c superconductors find a strong suppression of the integrated kinetic energy for the conduction electrons compared to that predicted by electronic band-structure calculations.¹⁷ A low carrier density in the cSDW phase of ferro-pnictide materials is consistent with quantum-oscillation experiments^{18,19} and with angle-resolved photoemission studies²⁰ that find evidence for tiny 2D Fermi-surface “spots”, each

on the order of 1% of the Brillouin zone. Also, the dependence on temperature shown by the electrical resistance of such parent compounds indicates proximity to a metal-insulator transition.²¹ Undoped ferro-pnictide materials in the cSDW phase then may very well lie near a Mott transition, where conduction electrons experience moderately strong repulsive interactions. By continuity with the limit of strong inter-electron repulsion, we therefore believe that a local-moment description of magnetism in parent compounds to iron-based high- T_c superconductors is a justifiable starting point at low temperature. The absence of a Stoner continuum of incoherent magnetic excitations reported in recent experimental studies of magnetic excitations in the cSDW phase of a ferro-pnictide material is consistent with this view.¹⁴ Consider then the following multi-orbital spin-1/2 Hamiltonian that contains near-neighbor Heisenberg exchange among local iron moments within isolated layers in addition to Hund's-rule coupling:⁷

$$H = \frac{1}{2}J_0 \sum_i \left[\sum_{\alpha} \mathbf{S}_i(\alpha) \right]^2 + \sum_{\langle i,j \rangle} \sum_{\alpha,\beta} J_1^{\alpha,\beta} \mathbf{S}_i(\alpha) \cdot \mathbf{S}_j(\beta) + \sum_{\langle\langle i,j \rangle\rangle} \sum_{\alpha,\beta} J_2^{\alpha,\beta} \mathbf{S}_i(\alpha) \cdot \mathbf{S}_j(\beta). \quad (1)$$

Above, $\mathbf{S}_i(\alpha)$ is the spin operator that acts on the spin-1/2 state of orbital α in the iron atom at site i . The latter runs over the square lattice of iron atoms that make up an isolated layer. The application of Hund's rule is controlled by a local ferromagnetic Heisenberg exchange constant $J_0 < 0$, while nearest neighbor and next-nearest neighbor Heisenberg exchange across the links $\langle i,j \rangle$ and $\langle\langle i,j \rangle\rangle$ is controlled by the tensor exchange constants $J_1^{\alpha,\beta}$ and $J_2^{\alpha,\beta}$, respectively. The strength of the crystal field at each iron atom determines the number of orbitals per iron atom above. It can be as low as two for strong crystal fields compared to the Hund's-rule coupling, in which case spin-1/2 moments exist on the iron $3d_{xz}$ and $3d_{yz}$ orbitals.^{4,22} Four $3d$ orbitals per iron atom carry spin-1/2 moments in the case of weak crystal fields compared to the Hund's-rule coupling, on the other hand.^{3,7} Last, the above model Hamiltonian reduces to the conventional J_1 - J_2 model over the square lattice when Hund's rule is enforced,^{8,9,13} $-J_0 \rightarrow \infty$, where the spin at each site is given by half the number of orbitals, $S = 1$ or $S = 2$.

We now illustrate a useful transformation of the model Hamiltonians (1) over the square lattice that relates eigenstates and eigenvalues with different nearest-neighbor Heisenberg exchange coupling constants. Let p denote a permutation of the orbitals. Consider then the partial "reflection" $P_{A(B)}$:

$$\text{orbital } \alpha \rightarrow p(\alpha) \quad \text{on the } A(B) \text{ sublattice} \quad (2)$$

of the Néel state. If Ψ is an eigenstate of the original model Hamiltonian (1) with energy E , the transformed state $\Psi' = P_{A(B)}\Psi$ is clearly then an eigenstate of the transformed Hamiltonian $H' = P_{A(B)}HP_{A(B)}^{-1}$ with energy E . Importantly, the Heisenberg exchange coupling constants transform under (2) as

$$J_1^{\alpha,\beta} \rightarrow J_1^{p(\alpha),\beta} \quad \text{and} \quad J_2^{\alpha,\beta} \rightarrow J_2^{p(\alpha),p(\beta)} \quad (3)$$

when orbital α lies on the $A(B)$ sublattice of the Néel state. Both $J_2^{\alpha,\beta}$ on the $B(A)$ sublattice and the Hund's rule coupling J_0 remain fixed. Yet how does the spectrum of states transform under (2)? Let T_x and T_y denote translations along the x axis and along the y axis by one lattice constant a . Because $T_x T_y$ moves each sublattice to itself, it commutes with P_A and with P_B . If Ψ has a crystal momentum $\hbar \mathbf{k}$, we therefore have that $T_x T_y \Psi' = e^{i(k_x + k_y)a} \Psi'$. The crystal momentum then transforms under (2) as

$$\mathbf{k} \rightarrow \mathbf{k} \text{ or } \mathbf{k} + (\pi/a, \pi/a). \quad (4)$$

Also, the spin of the new state Ψ' remains unchanged because P_A and P_B both commute with $\mathbf{S}_i = \sum_{\alpha} \mathbf{S}_i(\alpha)$.

It is also useful to consider the special case where all nearest-neighbor and next-nearest-neighbor exchange coupling constants are equal, respectively: $J_1^{\alpha,\beta} = J_1$ and $J_2^{\alpha,\beta} = J_2$. The model Hamiltonian (1) then reduces to $H = \frac{1}{2}J_0 \sum_i \mathbf{S}_i \cdot \mathbf{S}_i + J_1 \sum_{\langle i,j \rangle} \mathbf{S}_i \cdot \mathbf{S}_j + J_2 \sum_{\langle\langle i,j \rangle\rangle} \mathbf{S}_i \cdot \mathbf{S}_j$. Because $\mathbf{S}_i + \mathbf{S}_j$ commutes with $\mathbf{S}_i \cdot \mathbf{S}_i$, the latter then commutes with the Hamiltonian. The total spin at a given site i is hence a good quantum number. This means that the groundstate obeys Hund's rule in the classical limit because states with maximum total spin at a given site minimize both the Hund's-rule energy ($J_0 < 0$) and the Heisenberg exchange energies in such a case. A violation of Hund's rule will therefore require some variation in the Heisenberg exchange coupling constants among the different iron orbitals.

III. SPIN-1 IRON ATOMS

The iron 3d orbitals in ferro-pnictide materials experience a crystal field due to the neighboring pnictide atoms that lie above/below the center of each unit square of iron atoms. Both DFT calculations and basic considerations indicate that the crystal field splits these levels so that the degenerate $3d_{xz}$ and $3d_{yz}$ orbitals lie just below the highest-energy $3d$ orbital.^{4,22} The

Pauli principle then implies that spin $s = \hbar/2$ moments exist on both the $3d_{xz}$ and the $3d_{yz}$ orbitals in the limit of weak Hund's rule coupling. Henceforth, we shall assume that only two spin-1/2 orbitals, a and b , exist per iron atom in parent compounds to ferro-pnictide high- T_c superconductors. This is consistent with the ordered moment of $2\mu_B$ obtained by DFT calculations for antiferromagnetic groundstates of ferro-pnictide parent compounds.^{4,5,6} Let us next fix notation by assuming unique diagonal and unique off-diagonal Heisenberg exchange coupling constants over the nearest neighbor and the next-nearest neighbor links of the square lattice of iron atoms:

$$J_{1(2)}^{a,a} = J_{1(2)}^{\parallel} = J_{1(2)}^{b,b} \quad \text{and} \quad J_{1(2)}^{a,b} = J_{1(2)}^{\perp} = J_{1(2)}^{b,a}. \quad (5)$$

The author and Rezayi have recently shown that strong enough off-diagonal frustration, $J_2^{\perp} > 0$, can lead to either hidden ferromagnetic order or to hidden Néel order among spin-1/2 moments that are governed by the J_0 - J_1 - J_2 model Hamiltonian¹⁰ (1). Figure 1 displays the two types of hidden order, both of which show no net magnetic moment. Proximity of the collinear antiferromagnetic state, which exists at $J_2 > |J_1|/2$ when Hund's rule is enforced, to such hidden order can therefore account for the low ordered moment that is observed by elastic neutron diffraction in the cSDW state that exists at low temperature in undoped ferro-pnictide materials.² Balancing the energy of such hidden-order groundstates in the classical limit, $s \rightarrow \infty$, against that of conventional magnetic order leads to critical values for the Hund's rule coupling that are listed in Table I. True magnetic order becomes unstable to hidden magnetic order at weaker Hund's-rule coupling, $-J_0 < -J_{0c}$. A true magnetically ordered groundstate therefore first becomes unstable to the hidden-order groundstate that has the larger of the two critical values for the Hund's rule coupling strength, $-J_{0c}$. By Table I, for example, the true cSDW state becomes unstable to hidden ferromagnetic order at weak Hund's rule coupling only if the off-diagonal nearest-neighbor Heisenberg exchange is larger than the corresponding diagonal exchange: $J_1^{\perp} > J_1^{\parallel}$.

Linear Spin-Wave Theory. Study of the classical limit, $s \rightarrow \infty$, therefore indicates that extremely low ordered moments are possible at weak enough Hund's rule coupling, $J_0 < 0$, when off-diagonal frustration exists: $J_2^{\perp} > 0$. The nature of spin-wave excitations about the hidden magnetic order that is shown in Fig. 1 can also be obtained from the classical limit. In such case, each spin-1/2 moment obeys the following dynamical equation for precession:

$$\dot{\mathbf{S}}_i(\alpha) = \left[\frac{\partial H}{\partial \mathbf{S}_i(\alpha)} - \mathbf{h}_i(\alpha) \right] \times \mathbf{S}_i(\alpha). \quad (6)$$

HIDDEN FERROMAGNETIC ORDER

HIDDEN NEEL ORDER

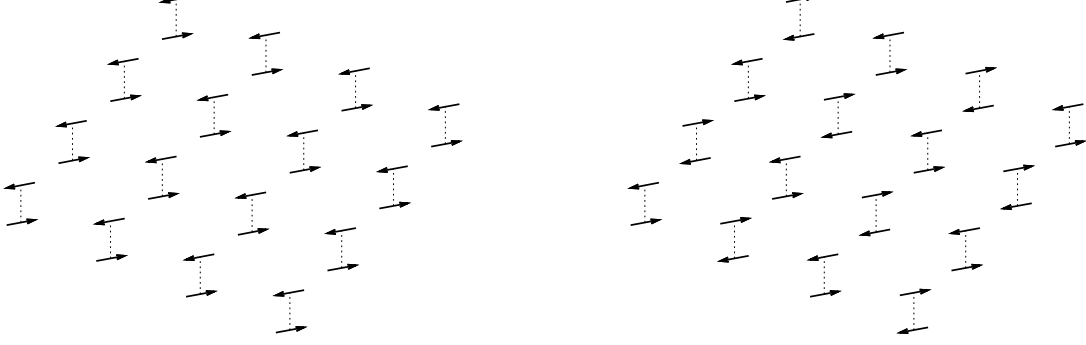


FIG. 1: Shown are two groundstates of a square lattice of spin-1 iron atoms that violate Hund's rule, but that exhibit hidden magnetic order. [See Eq. (1) and Table I.]

	True cSDW	True Néel	True Ferromagnet
Hidden Ferromagnet	$-J_{0c} = 2(J_1^\perp - J_1^\parallel) - 4J_2^\parallel$	$-J_{0c} = 4J_2^\perp - 4J_1^\parallel$	$-J_{0c} = 4J_2^\perp + 4J_1^\perp$
Hidden Néel	$-J_{0c} = 2(J_1^\parallel - J_1^\perp) - 4J_2^\parallel$	$-J_{0c} = 4J_2^\perp - 4J_1^\perp$	$-J_{0c} = 4J_2^\perp + 4J_1^\parallel$

TABLE I: Listed are the phase boundaries that separate true magnetic order from hidden magnetic order. The critical Hund's rule coupling is obtained by balancing the classical energies of the model Hamiltonian (1).

Here we have applied a magnetic field to the system, $\mathbf{h}_i(\alpha)$, that is in principle sensitive to the orbital degree of freedom, $\alpha = a$ or b . If the external magnetic field is a plane-wave with wavenumbers \mathbf{k} and frequency ω , then its transverse component with respect to the spin axis for hidden magnetic order generates a corresponding linear response in the transverse

components of the electronic spin. It has the form

$$\mathbf{S}_\perp(\pm, \mathbf{k}, \omega) = \chi_\perp(\pm, \mathbf{k}, \omega) \mathbf{h}_\perp(\pm, \mathbf{k}, \omega) \quad (7)$$

and

$$\mathbf{S}_\perp(\mp, \mathbf{k}, \omega) = i\bar{\chi}_\perp(\mathbf{k}, \omega) \mathbf{n}_\parallel \times \mathbf{h}_\perp(\pm, \mathbf{k}, \omega) \quad (8)$$

in the case of the hidden ferromagnetic state. Here we define true (+) and hidden (−) magnetic moments and magnetic fields by $\mathbf{S}(\pm) = \mathbf{S}(a) \pm \mathbf{S}(b)$ and by $\mathbf{h}(\pm) = [\mathbf{h}(a) \pm \mathbf{h}(b)]/2$, while \mathbf{n}_\parallel denotes the unit vector parallel to the magnetization axis for hidden order. Recall that the hidden ferromagnet is actually an antiferromagnet over the two sublattices set by the two orbitals a and b (see Fig. 1 and ref.²³). The true magnetic susceptibility, $\chi_\perp(+, \mathbf{k}, \omega)$, the hidden magnetic susceptibility, $\chi_\perp(-, \mathbf{k}, \omega)$, and the conjugate susceptibility $\bar{\chi}_\perp(\mathbf{k}, \omega)$ can then be obtained by solving the linear precession equation (6) that results in terms of the four transverse spin components per site, $\mathbf{S}_\perp(a)$ and $\mathbf{S}_\perp(b)$. This yields

$$\chi_\perp(\pm, \mathbf{k}, \omega) = s \frac{\Omega_\mp}{(\Omega_+ \Omega_-)^{1/2}} ([\omega + (\Omega_+ \Omega_-)^{1/2}]^{-1} - [\omega - (\Omega_+ \Omega_-)^{1/2}]^{-1}) \quad (9)$$

and

$$\bar{\chi}_\perp(\mathbf{k}, \omega) = s \frac{\omega}{(\Omega_+ \Omega_-)^{1/2}} ([\omega + (\Omega_+ \Omega_-)^{1/2}]^{-1} - [\omega - (\Omega_+ \Omega_-)^{1/2}]^{-1}), \quad (10)$$

with frequencies given by

$$\begin{aligned} \Omega_- &= s(J_1^\perp - J_1^\parallel) \sum_{n=x,y} (2 \sin \frac{1}{2} k_n a)^2 + s(J_2^\perp - J_2^\parallel) \sum_{n=+,-} (2 \sin \frac{1}{2} k_n a)^2 \\ \Omega_+ &= 2sJ_0 + sJ_1^\perp \sum_{n=x,y} (2 \cos \frac{1}{2} k_n a)^2 - sJ_1^\parallel \sum_{n=x,y} (2 \sin \frac{1}{2} k_n a)^2 \\ &\quad + sJ_2^\perp \sum_{n=+,-} (2 \cos \frac{1}{2} k_n a)^2 - sJ_2^\parallel \sum_{n=+,-} (2 \sin \frac{1}{2} k_n a)^2 \end{aligned}$$

in the case of the hidden ferromagnetic state. Above, $k_\pm = k_x \pm k_y$, a denotes the square lattice constant, and s is the electron spin $\hbar/2$. Next observe that the hidden Néel state is related to the hidden ferromagnetic state by the transformation (2) mentioned in the previous section. (See Fig. 1.) By (3), the frequencies Ω_\pm in that case are therefore obtained from the ones listed above for the hidden ferromagnet after making the exchange of the nearest-neighbor Heisenberg coupling constants, $J_1^\parallel \leftrightarrow J_1^\perp$. Further, the wavenumbers of the hidden spin $\mathbf{S}(-)$ and of the hidden magnetic field $\mathbf{h}(-)$ that appear in the linear-response equations (7) and (8) must be replaced by the wave numbers on the antiferromagnetic sublattice, $\mathbf{k} \rightarrow$

$\mathbf{k} - (\pi/a, \pi/a)$. The wavenumbers of the true spin and of the true magnetic field that appear there remain unchanged, however. The end result is that the true magnetic susceptibility $\chi_{\perp}(+, \mathbf{k}, \omega)$ in the hidden Néel state is given by that in the hidden ferromagnetic phase with the exchange $J_1^{\parallel} \leftrightarrow J_1^{\perp}$ alone, whereas the hidden magnetic susceptibility $\chi_{\perp}(-, \mathbf{k}, \omega)$ there is given by that in the hidden ferromagnetic phase with the previous exchange along with the replacement $\mathbf{k} \rightarrow \mathbf{k} + (\pi/a, \pi/a)$ in the wave numbers. [Cf. Eq. (4).]

Equation (9) and the discussion above yield true static magnetic susceptibilities $\chi_{\perp}(0) = (J_0 + 4J_1^{\perp} + 4J_2^{\perp})^{-1}$ for the hidden ferromagnetic state and $\chi_{\perp}(0) = (J_0 + 4J_1^{\parallel} + 4J_2^{\perp})^{-1}$ for the hidden Néel state. It also yields static susceptibilities for hidden magnetic order given by $\chi_{\perp}(-, \mathbf{k}, 0) = 2s/\Omega_{-}$, which correctly diverge as \mathbf{k} approaches the wavenumber that corresponds to either long-range ferromagnetic or Néel order. Finally, the poles of the dynamical susceptibility for hidden magnetic order (9), $\chi_{\perp}(-, \mathbf{k}, \omega)$, represent two spin-wave excitations of momentum $\hbar\mathbf{k}$ that correspond to the two possible orientations of the transverse component of the hidden moment, $\mathbf{S}_{\perp}(-, \mathbf{k}, \omega)$. They both lie at an energy $\hbar(\Omega_{+}\Omega_{-})^{1/2}$ above the groundstate energy. These spin-wave excitations are also reflected by the poles in the dynamical susceptibility for true magnetic order (9), $\chi_{\perp}(+, \mathbf{k}, \omega)$. As mentioned above, however, the wave number \mathbf{k} shifts by the characteristic amount $(\pi/a, \pi/a)$ in the case of hidden Néel order. Last, both spinwaves have spectral weights

$$A(\pm, \mathbf{k}) = \pi s(\Omega_{\mp}/\Omega_{\pm})^{1/2} \quad (11)$$

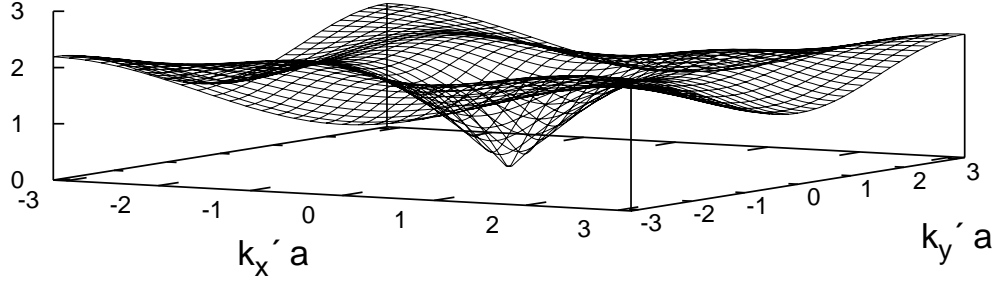
in the true (+) and the hidden (−) channels that are read off from the imaginary part of the dynamical susceptibility:

$$\text{Im } \chi_{\perp}(\pm, \mathbf{k}, \omega) = A(\pm, \mathbf{k})(\delta[\omega - (\Omega_{+}\Omega_{-})^{1/2}] - \delta[\omega + (\Omega_{+}\Omega_{-})^{1/2}]). \quad (12)$$

The peaks in the dynamical structure function above signal spin-wave excitations that are observable by inelastic neutron scattering only in the true magnetic (+) channel. Recalling the discussion following Eq. (9), the true dynamical susceptibility $\chi_{\perp}(+, \mathbf{k}, \omega)$ is common to a hidden ferromagnet and to a hidden Néel state that are related by the transformation (2). Inelastic neutron scattering is therefore unable to discriminate between these two possible types of hidden magnetic order!

Figure 2 depicts the linear spin-wave spectrum for a cSDW with intervening hidden ferromagnetic (Néel) order at two extreme values for the Hund’s rule coupling: absent and

SPIN-WAVE EXCITATION ENERGY IN ABSENCE OF HUND'S RULE COUPLING



SPIN-WAVE EXCITATION ENERGY AT TRANSITION INTO HIDDEN MAGNETIC ORDER

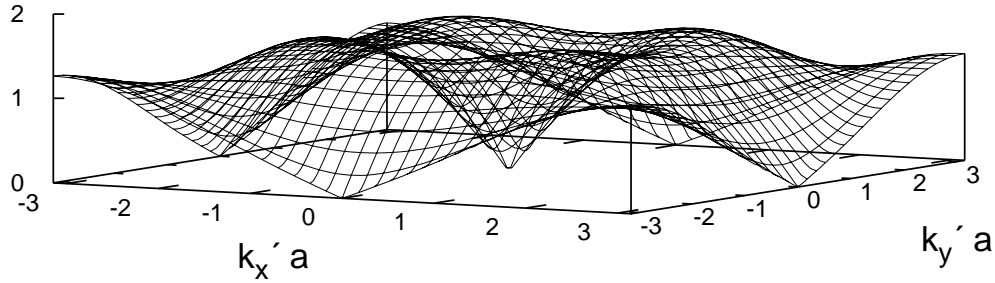


FIG. 2: Displayed is the linear spin-wave spectrum of the Hamiltonian (1) for the following set of Heisenberg exchange coupling constants: $J_1^{||(\perp)} = 0$, $J_1^{\perp(||)} > 0$, and $J_2^{||} = 0.3 J_1^{\perp(||)} = J_2^{\perp}$. The Hund's rule coupling at the quantum critical point that separates hidden ferromagnetic (Néel) order from a cSDW is set by the value listed in Table I. Spin-wave energies are given in units of $\hbar^2 J_1^{\perp(||)}$ and the wavenumber \mathbf{k}' is associated with the antiferromagnetic sublattice for hidden order. (See Fig. 1.)

critical. Here, we have chosen Heisenberg exchange coupling constants $J_1^{||(\perp)} = 0$, $J_1^{\perp(||)} > 0$, and $J_2^{||} = 0.3 J_1^{\perp(||)} = J_2^{\perp}$, which lies near maximum frustration when Hund's rule is obeyed. The top graph displays how the spectrum collapses linearly to the groundstate energy at zero momentum in the absence of Hund's rule coupling. In general, the spin-wave velocity is given by

$$v_0 = 2sa([J_1^{\perp} - J_1^{||} + 2(J_2^{\perp} - J_2^{||})] \cdot [\frac{1}{2}J_0 + 2J_1^{\perp} + 2J_2^{\perp}])^{1/2} \quad (13)$$

in the hidden ferromagnet, and by the same expression after the exchange (2) $J_1^{||} \leftrightarrow J_1^{\perp}$ in the hidden Néel state. It correctly collapses to zero at the phase boundary with the true ferromagnetic state by Table I, at which point the spin-wave excitation frequency disperses

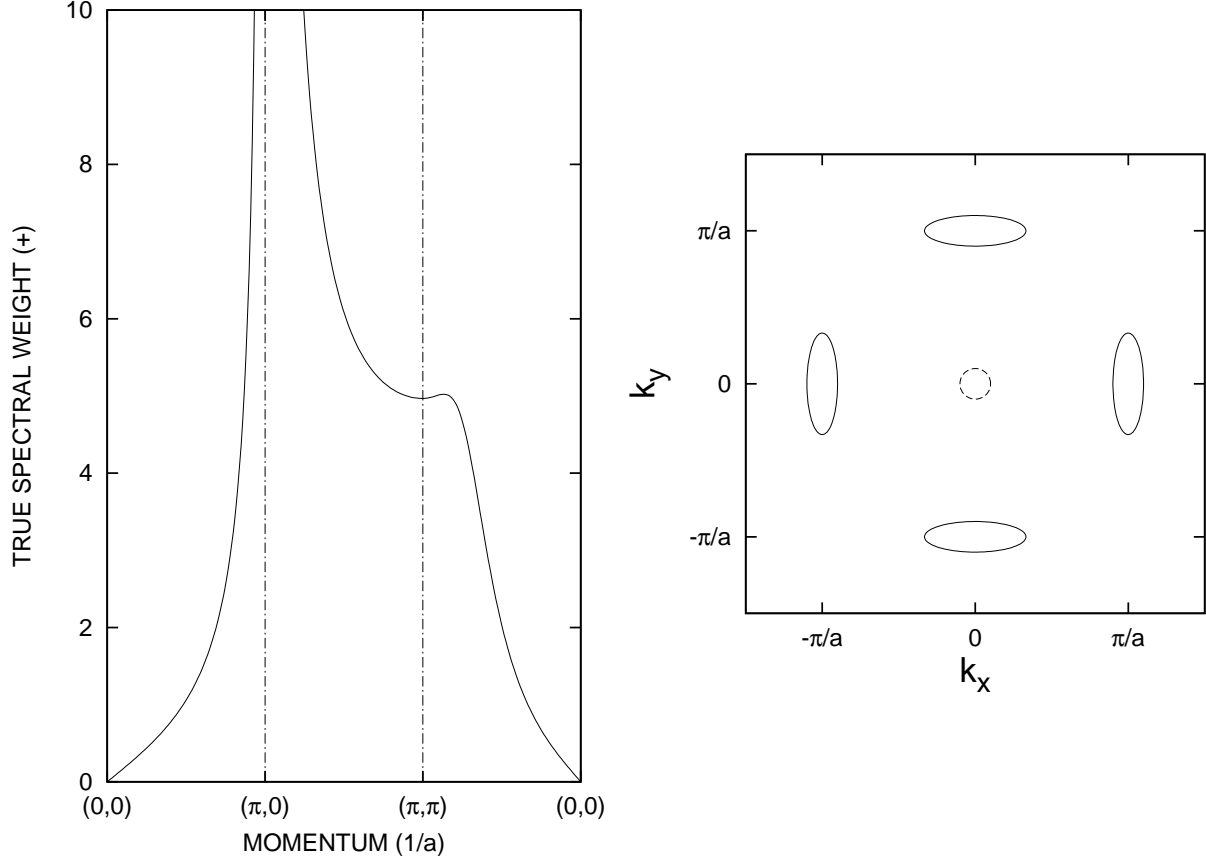


FIG. 3: The spectral weight of observable (+) spinwaves at the quantum critical point that separates hidden ferromagnetic (Néel) order from a cSDW is shown in units of \hbar . The following set of Heisenberg exchange coupling constants are used: $J_1^{\parallel(\perp)} = 0$, $J_1^{\perp(\parallel)} > 0$, and $J_2^{\parallel} = 0.3 J_1^{\perp(\parallel)} = J_2^{\perp}$. The critical Hund's rule exchange coupling is set to the value listed in Table I. Also shown are contours over the Brillouin zone for such spinwaves at a low fixed excitation energy.

quadratically with wavenumber. Notice, however, the mild depression in the top spectrum that is centered at the cSDW wave number $\mathbf{k}_{cSDW} = (\pi/a, 0)$. The bottom graph in Fig. 2 shows how it softens completely to zero energy at the critical value for Hund's rule coupling, $-J_{0c} = 0.8 J_1^{\perp(\parallel)}$, in which case the hidden ferromagnetic (Néel) state transits into the cSDW state by Table I. These special zero-energy modes result from the collapse of the frequency $\Omega_+(\mathbf{k}_{cSDW})$ to zero there. Evaluating $(\Omega_+ \Omega_-)^{1/2}$ at \mathbf{k}_{cSDW} from the expressions for the frequencies that are listed below Eq. (10) yields the spin gap there:

$$\Delta_{cSDW} = 2s[(4J_2^{\perp} - J_{0c})(J_0 - J_{0c})]^{1/2}. \quad (14)$$

The former also implies a divergent spectral weight (11) for such spinwaves at the quantum

phase transition:

$$A(+, \mathbf{k}_{cSDW}) = \pi s[(4J_2^\perp - J_{0c})/(J_0 - J_{0c})]^{1/2}. \quad (15)$$

Because inelastic neutron scattering is proportional to $\text{Im } \chi_\perp(+, \mathbf{k}, \omega)$, low-energy spin-waves with momentum near $\hbar \mathbf{k}_{cSDW}$ will dominate such measurements near the transition between the cSDW state and hidden magnetic order (see Fig. 3). Study of the expressions for the frequencies Ω_\pm that are listed below Eq. (10) yields that the dominant spin-wave excitations centered at the cSDW wave numbers \mathbf{k}_{cSDW} disperse up from the groundstate energy as $[v_l^2(k_l - \pi/a)^2 + v_t^2 k_t^2 + \Delta_{cSDW}^2]^{1/2}$ in general. (See Fig. 2.) Here k_l and k_t are the components of \mathbf{k} that are respectively parallel and perpendicular to \mathbf{k}_{cSDW} . Near criticality, $\Delta_{cSDW} \rightarrow 0$, the cSDW order is short range, with correlations lengths $\xi_{cSDW}^{(l)} = v_l/\Delta_{cSDW}$ and $\xi_{cSDW}^{(t)} = v_t/\Delta_{cSDW}$ in the longitudinal and transverse directions. At criticality, $\Delta_{cSDW} = 0$, the longitudinal velocity v_l coincides with the spin-wave velocity v_0 for hidden magnetic order (13), while the transverse velocity v_t is equal to the previous divided by the anisotropy parameter

$$\frac{v_l}{v_t} = \left[\frac{2(J_2^\parallel + J_2^\perp) + J_1^\parallel + J_1^\perp}{2(J_2^\parallel + J_2^\perp) - J_1^\parallel - J_1^\perp} \right]^{1/2}. \quad (16)$$

The latter coincides with the anisotropy of low-energy spinwaves that is predicted by the conventional J_1 - J_2 model, in which case $J_{1(2)} = [J_{1(2)}^\parallel + J_{1(2)}^\perp]/2$ by Hund's rule.

Exact Diagonalization. The above semi-classical analysis indicates that large enough off-diagonal frustration can induce a quantum phase transition into hidden magnetic order that is unfrustrated, but that violates Hund's rule. We shall now confirm this by obtaining the exact low-energy spectrum of states for the J_0 - J_1 - J_2 model (1) with two spin-1/2 moments per site over a 4 by 4 square lattice with periodic boundary conditions. The model Hamiltonian operator (1) acts on a Hilbert space that is restricted to have 16 up spins and 16 down spins. Next, translational invariance is exploited in order to bring H into block-diagonal form. Each block of the Hamiltonian is labeled by the allowed momentum quantum numbers: $(k_x a, k_y a) = (0, 0), (\pi, 0), (\pi, \pi), (\pi/2, 0), (\pi/2, \pi/2)$ and $(\pi, \pi/2)$, plus their symmetric counterparts. Spin-flip symmetry is also exploited to further block-diagonalize the Hamiltonian at such momenta into two blocks that are respectively even and odd under it. The combination of translation and spin-flip symmetries reduces the dimension of each block to a little under 19,000,000 states. Next, we construct the Hamiltonian operator (1) over each of these subspaces. Every term in Hamiltonian (1) represents a Heisenberg spin exchange that

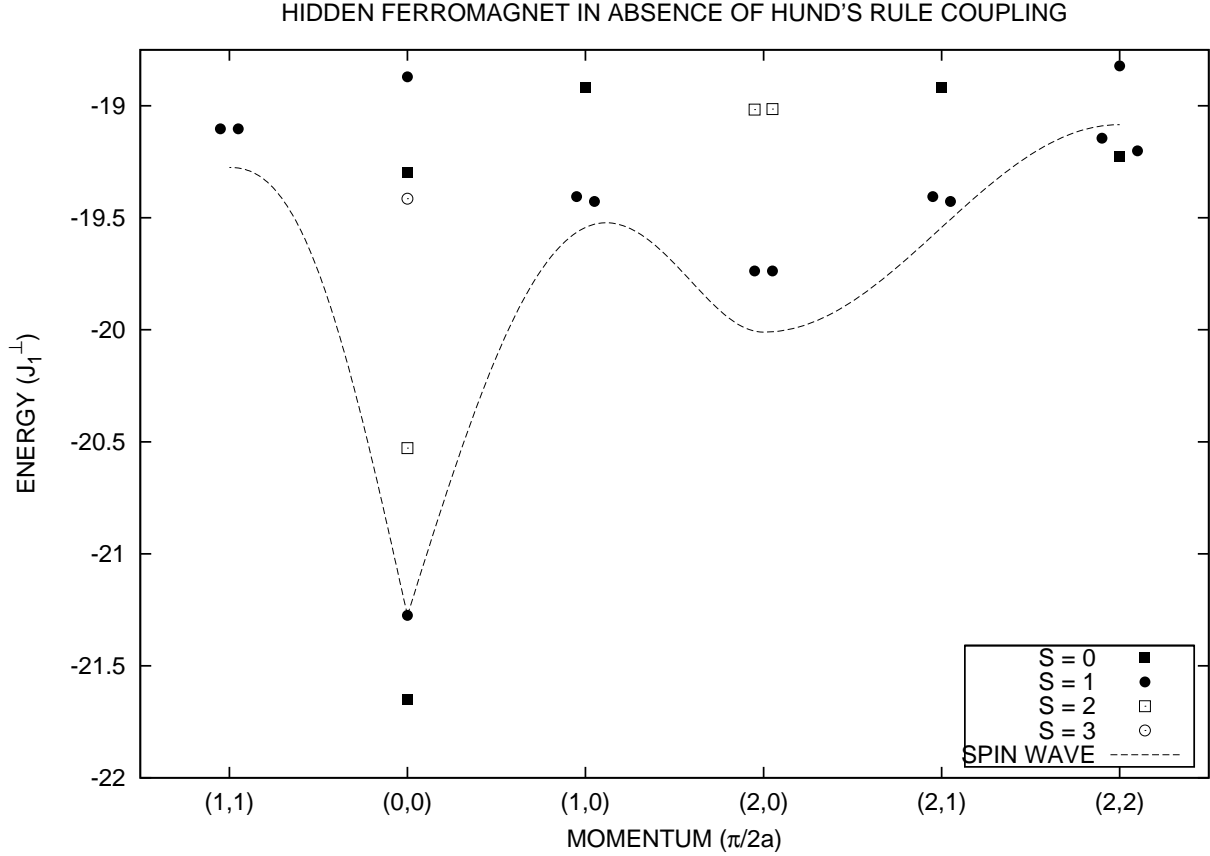


FIG. 4: Shown is the low-energy spectrum for $4 \times 4 \times 2$ spin-1/2 moments that experience the following set of Heisenberg exchange coupling constants: $J_0 = 0$, $J_1^\parallel = 0$, $J_1^\perp > 0$, and $J_2^\parallel = 0.3 J_1^\perp = J_2^\perp$. The lowest-energy spin-1 state at zero momentum is used as the reference for the linear spin-wave approximation. Hereafter, we set $\hbar \rightarrow 1$.

permutes the Bloch-wave type states. These permutations are stored in memory. Hamiltonian matrix elements that involve Bloch waves composed of configurations of spin up and spin down that display absolutely no non-trivial translation invariance up to a spin-flip are also stored in memory. They are calculated otherwise. Because the vast majority of Bloch waves lie in the first category, the Hamiltonian operator is stored in memory for all practical purposes. This speeds up its application on a given state tremendously. The application of the Hamiltonian H on a given state is accelerated further by enabling shared-memory parallel computation through OpenMP directives. Last, we apply the iterative Lanczos technique numerically over each subspace labeled by momentum and by spin-flip quantum numbers.²⁴ The ARPACK subroutine library is employed for this purpose.²⁵

Figures 4, 5 and 6 show how the low-energy spectrum of the J_0 - J_1 - J_2 model (1) evolves

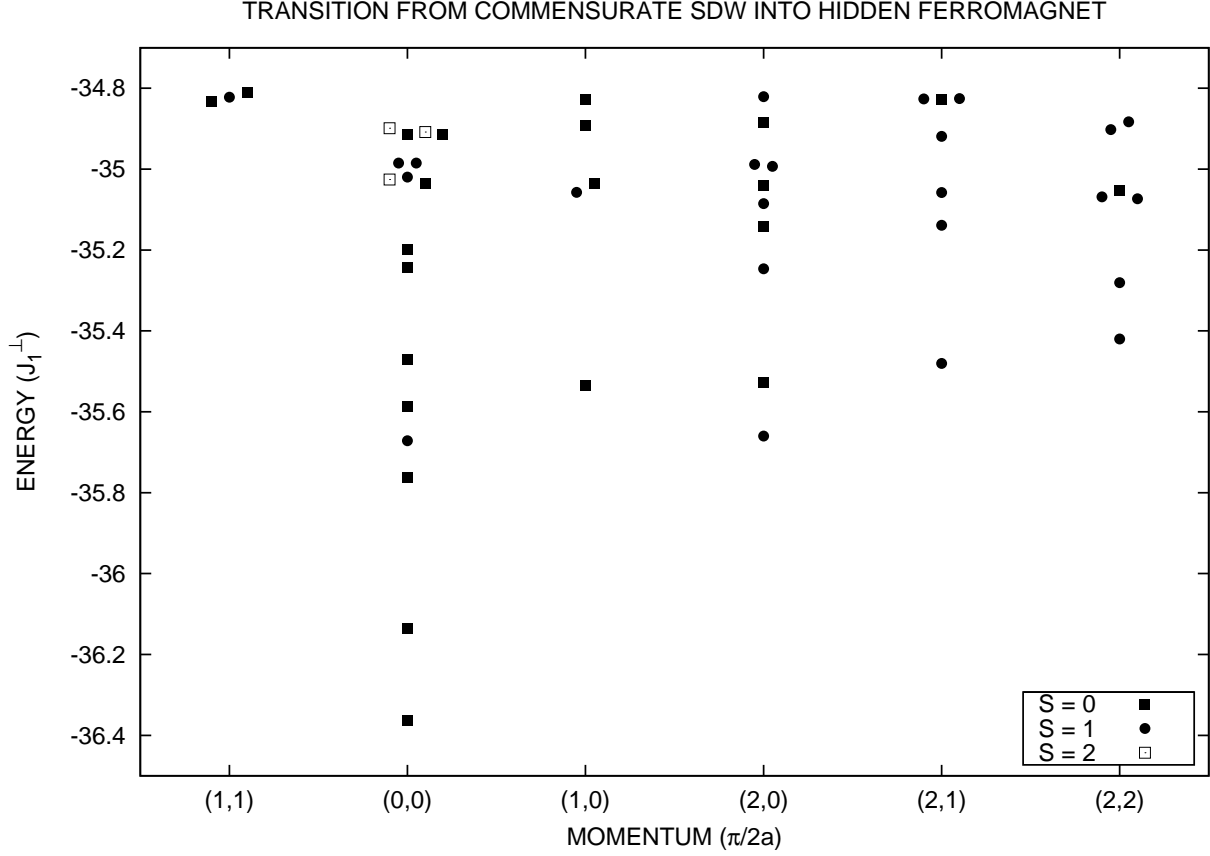


FIG. 5: Shown is the low-energy spectrum for $4 \times 4 \times 2$ spin-1/2 moments that experience the following set of Heisenberg exchange coupling constants: $J_1^\parallel = 0$, $J_1^\perp > 0$, and $J_2^\parallel = 0.3 J_1^\perp = J_2^\perp$. The Hund's rule exchange coupling is set to $J_0 = -1.35 J_1^\perp$.

with the strength of the Hund's rule coupling in the presence of off-diagonal frustration. The following Heisenberg exchange coupling constants were chosen: $J_1^\parallel = 0$, $J_1^\perp > 0$, and $J_2^\parallel = 0.3 J_1^\perp = J_2^\perp$. A hidden ferromagnetic state is then expected in the absence of Hund's rule coupling, while a cSDW is expected when Hund's rule is obeyed. In the former case displayed by Fig. 4, notice the coincidence between the linear spin-wave approximation about hidden-order, Eq. (12) and Fig. 2, and the present exact-diagonalization results. It indicates that the classical prediction of long-range hidden magnetic order holds true for spin-1/2 moments per iron orbital. Figure 6 displays the spectrum at strong Hund's rule coupling, $-J_0 = 15 J_1^\perp$, on the other hand. The bulk of the groundstate energy is due to the Hund's rule coupling, which is given by $16 J_0 = -240 J_1^\perp$ when Hund's rule is obeyed. Notice the low-energy spin-1 state at the cSDW wave number $(\pi/a, 0)$, as well as the softening of the spin-1 excited state at the wave number $(\pi/a, \pi/a)$ that characterizes the Néel state.

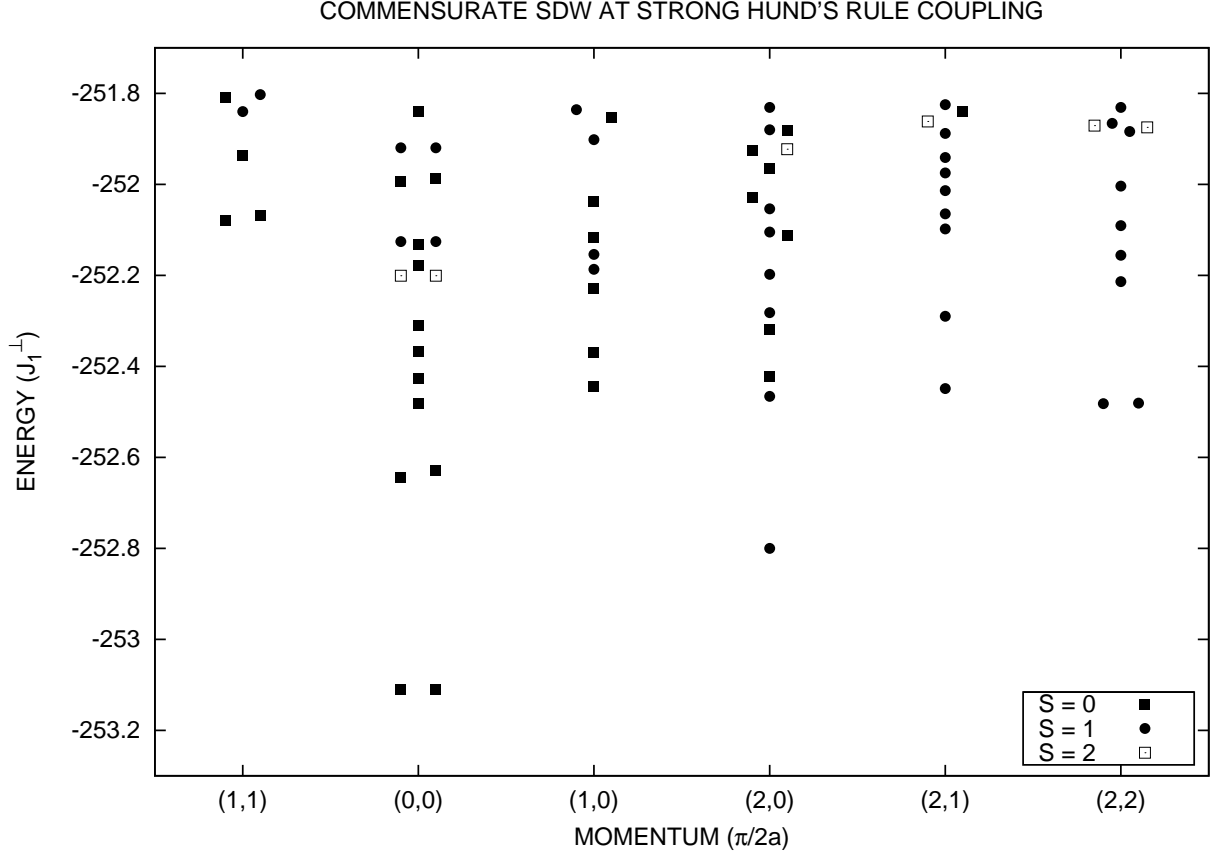


FIG. 6: The low-energy spectrum of the cSDW is obtained from exact diagonalization of $4 \times 4 \times 2$ spin-1/2 moments. The following set of Heisenberg exchange coupling constants are used: $J_1^\parallel = 0$, $J_1^\perp > 0$, $J_2^\parallel = 0.3 J_1^\perp = J_2^\perp$, and $J_0 = -15 J_1^\perp$.

The dispersion of these spin-1 excited states resembles the spin-wave spectrum predicted for the cSDW in the conventional J_1 - J_2 model, where Hund's rule is obeyed.^{13,14} Figure 6 also displays that the groundstate is doubly degenerate, which again is consistent with cSDW order over the square lattice. Last, Fig. 5 shows the low-energy spectrum for Hund's rule coupling $J_0 = -1.35 J_1^\perp$ near a possible quantum phase transition (cf. Fig. 7). The lowest-energy spin-1 excitations at momentum $(0,0)$ and $(\pi/a, 0)$ are degenerate, and their dispersion resembles the prediction from linear spin-wave theory that is shown by Fig. 2. Notably, the lowest-energy spin-1 excitation does *not* “dip down” at momentum $(\pi/a, \pi/a)$. Table I predicts a transition into hidden order at $J_0 = -0.8 J_1^\perp$ in the classical limit at large spin s , however, which suggests that quantum effects renormalize up the critical Hund's rule coupling in the physically relevant case of spin-1/2 iron $3d$ orbitals.

Figure 7 shows the evolution of relevant magnetic order parameters with Hund's rule

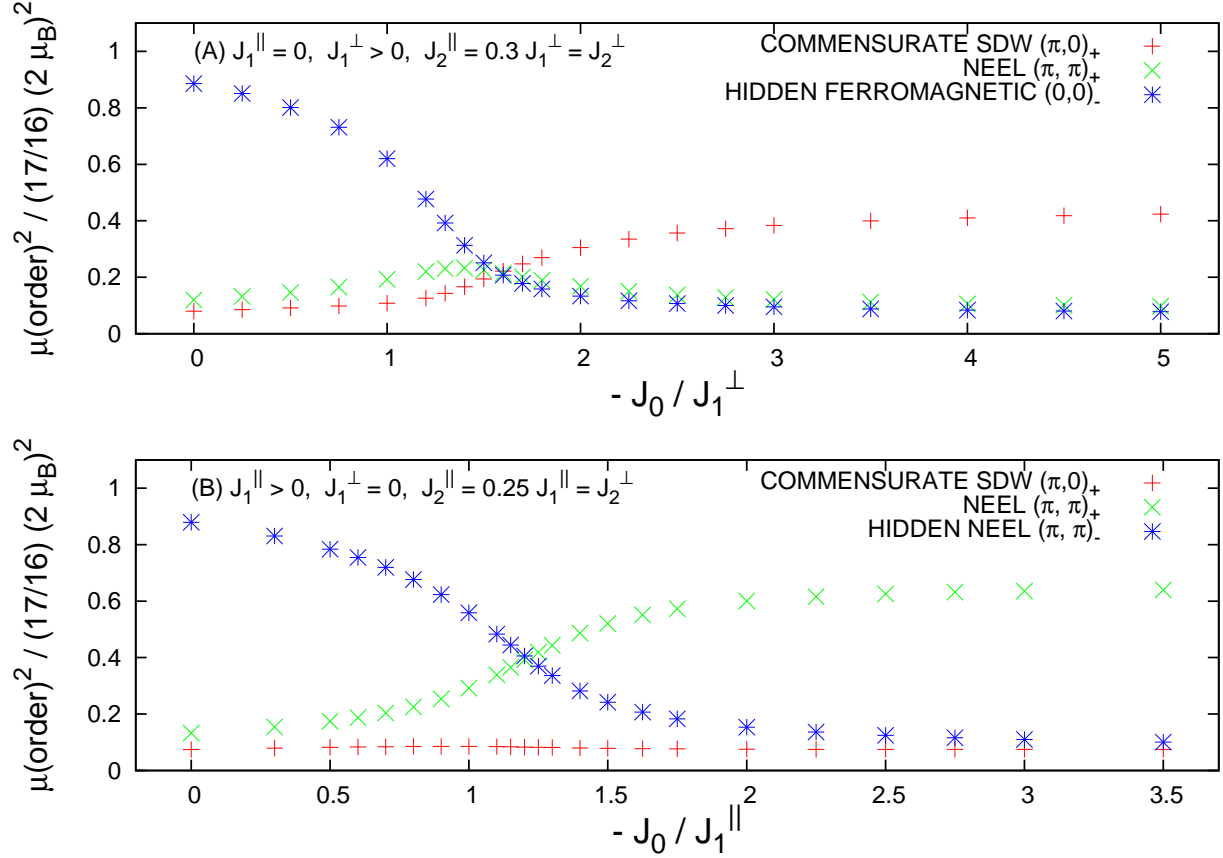


FIG. 7: Displayed is the autocorrelation of the order parameter (17) for true (+) and for hidden (-) magnetic order on a $4 \times 4 \times 2$ lattice of spin-1/2 moments as a function of Hund's rule coupling. It is normalized to its value in the true ferromagnetic state (see text).

coupling under the previous set of Heisenberg exchange coupling constants. Plotted on the vertical axis is the autocorrelation $\langle \mathbf{O}(\mathbf{k})_{\pm} \cdot \mathbf{O}(-\mathbf{k})_{\pm} \rangle_0$ of the order parameter

$$\mathbf{O}(\mathbf{k})_{\pm} = \sum_i e^{i\mathbf{k} \cdot \mathbf{r}_i} [\mathbf{S}_i(a) \pm \mathbf{S}_i(b)] \quad (17)$$

over the groundstate normalized to its value in the true ferromagnetic state, $\langle \mathbf{O}(0)_{+} \cdot \mathbf{O}(0)_{+} \rangle_0 = 16 \cdot 17 \hbar^2$. The relation to the ordered magnetic moment per iron atom, $\boldsymbol{\mu}(\pm, \mathbf{k})$, given there is obtained from the identity $|16 \boldsymbol{\mu}(\pm, \mathbf{k})|^2 = (2\mu_B/\hbar)^2 \langle \mathbf{O}(\mathbf{k})_{\pm} \cdot \mathbf{O}(-\mathbf{k})_{\pm} \rangle_0$ that is valid over the 4 by 4 square lattice of spin-1 iron atoms. The top graph in Fig. 7 displays how the square of the ordered moment for true cSDW order (+) decays with decreasing Hund's rule coupling. It notably accounts for the low ordered moment that is observed by elastic neutron diffraction in an undoped parent compound to the recently discovered ferro-pnictide high- T_c superconductors.² Also shown there is how hidden ferromagnetic order is

established once cSDW order fades away. Figure 7 then provides evidence for a quantum phase transition that separates a hidden ferromagnetic state at weak Hund's rule coupling from a cSDW state at strong Hund's rule coupling. Notice that the putative quantum phase transition at $J_0 \cong -1.35 J_1^\perp$ (see Fig. 5) occurs at a Hund's rule exchange coupling that is almost a factor-of-2 times larger than the classical prediction $J_{0c} = -0.8 J_1^\perp$ listed in Table I. Last, the bottom graph in Fig. 7 shows the evolution of the relevant order parameters in the case of true Néel order with intervening hidden Néel order. Here, we have chosen Heisenberg exchange coupling constants $J_1^\parallel > 0$, $J_1^\perp = 0$, and $J_2^\parallel = 0.25 J_1^\parallel = J_2^\perp$, which lies at maximum frustration when Hund's rule is obeyed. The common inflection point at $J_0 \cong -1.2 J_1^\parallel$ is consistent with a quantum phase transition at a value of Hund's rule coupling that is noticeably larger than the classical prediction of $J_{0c} = -J_1^\parallel$ listed in Table I.

IV. DISCUSSION AND CONCLUSIONS

Recent inelastic neutron scattering measurements on the parent compound to ferro-pnictide superconductors CaFe_2As_2 have uncovered well-defined spin-wave excitations in the cSDW phase throughout virtually the entire Brillouin zone.¹⁴ Instead of softening at the wavenumber $(\pi/a, \pi/a)$ that corresponds to Néel order as predicted by the conventional J_1 - J_2 model over the square lattice, they show a local maximum there. Figure 8 displays a fit of the spin-wave spectrum obtained by inelastic neutron scattering on CaFe_2As_2 to the prediction for the linear spin-wave dispersion of a square lattice of spin-1 iron atoms, $(\Omega_+ \Omega_-)^{1/2}$, at the quantum critical point that separates the cSDW phase from hidden ferromagnetic (Néel) order [see Eq. (12) and Fig. 2]. The spin per orbital is set to $s = 1/2$ and the following Heisenberg exchange coupling constants are used: $J_{0c} = -57.0$ meV, $J_1^{\parallel(\perp)} = 0$, $J_1^{\perp(\parallel)} = 115.8$ meV, and $J_2^\parallel = 43.7$ meV $= J_2^\perp$. These imply a ratio $J_2/J_1 = 0.75$ between the next-nearest-neighbor and the nearest-neighbor Heisenberg exchange constants deep inside the cSDW, where Hund's rule is obeyed. Notice that the measured spin-wave spectrum terminates before it reaches the predicted Goldstone modes at zero momentum that correspond to hidden magnetic order. This is consistent with Fig. 3, which displays how the spectral weight of low-energy spin-waves about zero momentum is dwarfed by that (15) of low-energy spinwaves about momentum $(\pi/a, 0)$ at the quantum critical point that separates the cSDW phase from hidden magnetic order.

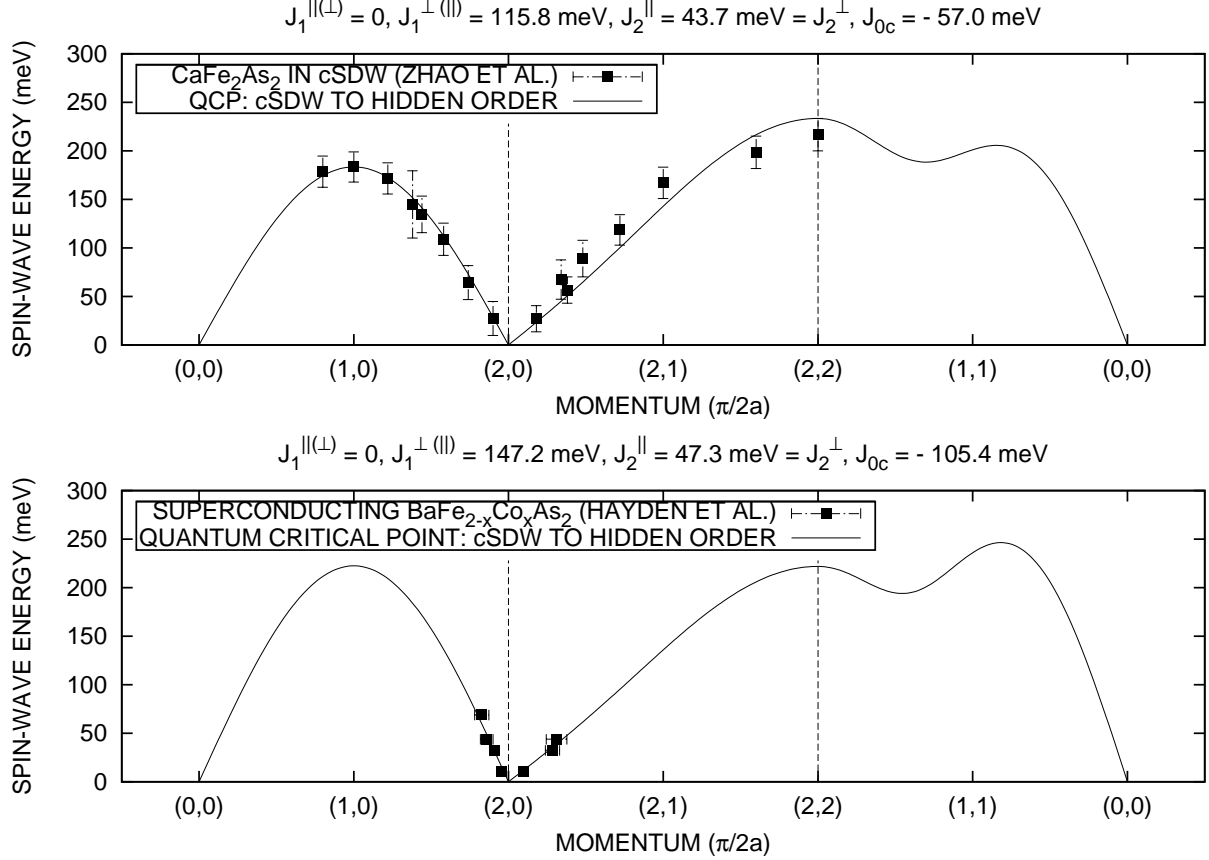


FIG. 8: The spin excitation spectra of two pnictide materials are fit to the linear spinwave spectrum expected at a quantum critical point (QCP) that separates a cSDW from ferromagnetic (Néel) hidden order. [See Eq. (12) and Fig. 2.] The wavenumber in the direction perpendicular to the planes of iron atoms corresponds to antiferromagnetic order in both sets of data. (See refs.¹⁴ and¹⁵.)

More recent inelastic neutron scattering measurements on the ferro-pnictide superconductor $\text{BaFe}_{2-x}\text{Co}_x\text{As}_2$ have uncovered low-energy spin-wave excitations that disperse *up* in energy in an anisotropic fashion away from the wavenumbers that correspond to cSDW order;¹⁵ e.g. $(\pi/a, 0)$. Paradoxically, no evidence for long-range magnetic order exists in this ferro-pnictide superconductor. Figure 8 displays a fit of the spin-wave spectrum obtained by inelastic neutron scattering on $\text{BaFe}_{2-x}\text{Co}_x\text{As}_2$ to the prediction for the linear spin-wave dispersion of a square lattice of spin-1 iron atoms, $(\Omega_+\Omega_-)^{1/2}$, at the quantum critical point that separates the cSDW phase from hidden ferromagnetic (Néel) order [see Eq. (12) and Fig. 2]. The spin per orbital is again set to $s = 1/2$, and the following Heisenberg exchange coupling constants are used: $J_{0c} = -105.4$ meV, $J_1^{\parallel(\perp)} = 0$, $J_1^{\perp(\parallel)} = 147.2$

meV, and $J_2^{\parallel} = 47.3 \text{ meV} = J_2^{\perp}$. This fit implies a ratio $J_2/J_1 = 0.64$ between the next-nearest-neighbor and the nearest-neighbor Heisenberg exchange constants deep inside the cSDW. Although the conventional J_1 - J_2 model over the square lattice can also account for the linear and anisotropic dispersion of the spinwaves that are observed in superconducting¹⁵ $\text{BaFe}_{2-x}\text{Co}_x\text{As}_2$, it cannot account for the absence of long-range magnetic order. Both the semi-classical analysis about hidden magnetic order and the exact diagonalization studies on a 4×4 lattice described in the previous section indicate, on the other hand, that the moment associated with true cSDW order is extremely small at the quantum critical point into hidden magnetic order. (See Figs. 1 and 7.)

In conclusion, a linear spin-wave analysis of the J_0 - J_1 - J_2 model Hamiltonian (1) that describes a square lattice of frustrated spin-1 iron atoms yields a quantum critical point as a function of Hund's rule exchange coupling ($-J_0$) that separates a cSDW from hidden ferromagnetic or hidden Néel order. The observable spectral weight of the Goldstone modes associated with hidden order is predicted to be small in general (see Fig. 3). A strong variation between the diagonal and the off-diagonal exchange couplings of the multi-orbital Heisenberg model (1) across nearest-neighbors *alone* is sufficient for Hund's rule to give way to hidden magnetic order. Recent DFT calculations obtain ferromagnetic direct exchange and antiferromagnetic superexchange across nearest-neighbor iron moments in the cSDW phase of ferro-pnictide materials.⁶ Their superposition potentially can result in the required difference between J_1^{\parallel} and J_1^{\perp} . Fits of the critical linear spin-wave spectrum to recent experimental studies of magnetic excitations in ferro-pnictide materials^{14,15} yield a Hund's rule exchange coupling constant on the order of 100 meV. Figure 7 displays the dependence of the ordered magnetic moments on Hund's rule coupling obtained from exact diagonalization of the model Hamiltonian (1) over a 4×4 lattice, with two spin-1/2 orbitals per site. The top graph implies a critical Hund's rule coupling at the transition between hidden ferromagnetic order and cSDW order that is almost twice the classical prediction listed in Table I: $-J_{0c} = 0.8 J_1^{\perp}$. Correcting for this discrepancy brings the value of the Hund's rule coupling closer to the estimate of 700 meV that is obtained for ferro-pnictides by dynamical mean field theory.²⁶ (Note that $-J_0$ is twice as big as the Hund's rule exchange coupling that appears naturally in multi-orbital Hubbard models.)

The success of the theoretical fits to the inelastic neutron scattering data displayed by Fig. 8 indicates that a local-moment picture for magnetism in ferro-pnictide materials is

valid. Whether magnetic moments in ferro-pnictide materials are itinerant or localized is vigorously debated, however. In particular, the metallic temperature dependence shown by the electrical resistance in the cSDW phase of ferro-pnictide materials in addition to the absence of satellite peaks in inelastic X-ray scattering spectra is consistent with itinerant magnetism.^{21,27} The multi-orbital Heisenberg model Hamiltonian (1) studied here is also potentially consistent with the semi-metallic nature of ferro-pnictide materials, on the other hand. Figure 1 indicates that the classical hidden ferromagnetic state remains intact in the presence of mobile holes that are prohibited from hopping between orbitals, for example. Likewise, the classical hidden Néel state remains intact in the presence of mobile holes that are restricted to hop between different orbitals at nearest-neighbor sites of the square lattice of iron atoms. Such limiting cases can result in low-energy electronic hole excitations near zero momentum, which are consistent with the electronic structure revealed by angle-resolved photoemission spectroscopy (ARPES) in the cSDW phase of ferro-pnictide materials.²⁸ Resonant scattering of such hole excitations with the quantum-critical spin-waves studied here (Figs. 2 and 3) could also result in low-energy single-particle excitations at momenta near those associated with cSDW order. Recent ARPES studies of BaFe_2As_2 in the cSDW phase reveal the existence of low-energy electronic excitations near such momenta.²⁰ The measured electronic spectrum there forms a Dirac cone, with a Fermi velocity of about 330 meV \AA . It is an order of magnitude smaller than in graphene, and it is hence consistent with strong electronic correlations.²⁹ It also remarkably lies inside the range of spin-wave velocities extracted from low-energy magnetic excitations near cSDW wave numbers in the doped superconducting compound $\text{BaFe}_{2-x}\text{Co}_x\text{As}_2$:¹⁵ $v_t = 230 \text{ meV \AA}$ and $v_l = 580 \text{ meV \AA}$ (see Fig. 8). The above observations therefore indicate that injecting mobile holes into the states studied here that display hidden magnetic order (Fig. 1) potentially can account for the nature of low-energy single-particle excitations in ferro-pnictide materials. They also indicate that a description of the superconducting state of ferro-pnictide materials in terms of a doped Mott insulator⁷ is possible.

Acknowledgments

The author thanks Ed Rezayi, Radi Al Jishi and Elena Bascones for useful discussions. Exact diagonalizations of the J_0 - J_1 - J_2 model (1) were carried out on the SGI Altix 4700

(Hawk) at the AFRL DoD Supercomputer Resource Center. This work was supported in part by the US Air Force Office of Scientific Research under grant no. FA9550-09-1-0660.

- ¹ Y. Kamihara, T. Watanabe, M. Hirano, and H. Hosono, J. Am. Chem. Soc. **130**, 3296 (2008)
- ² C. de la Cruz, Q. Huang, J.W. Lynn, J. Li, W. Ratcliff, J.L. Zarestky, H.A. Mook, G.F. Chen, J.L. Luo, N.L. Wang and P. Dai, Nature **453**, 899 (2008).
- ³ K. Haule, J.H. Shim, and G. Kotliar, Phys. Rev. Lett. **100**, 226402 (2008).
- ⁴ Chao Cao, P. J. Hirschfeld and Hai-Ping Cheng, Phys. Rev. B **77**, 220506(R) (2008).
- ⁵ J. Dong, H. J. Zhang, G. Xu, Z. Li, G. Li, W. Z. Hu, D. Wu, G. F. Chen, X. Dai, J. L. Luo, Z. Fang, N. L. Wang, Euro. Phys. Lett. **83**, 27006 (2008).
- ⁶ F. Ma, Z.-Y. Lu and T. Xiang, Phys. Rev. B **78**, 224517 (2008).
- ⁷ Q. Si and E. Abrahams, Phys. Rev. Lett. **101**, 076401 (2008).
- ⁸ P. Chandra and B. Doucot, Phys. Rev. B **38**, 9335 (1988).
- ⁹ Burkhard Schmidt, Mohammad Siahatgar, Peter Thalmeier, Phys. Rev. B **81**, 165101 (2010).
- ¹⁰ J.P. Rodriguez and E.H. Rezayi, Phys. Rev. Lett. **103**, 097204 (2009).
- ¹¹ J. Zhao, D.-X. Yao, S. Li, T. Hong, Y. Chen, S. Chang, W. Ratcliff, J. W. Lynn, H. A. Mook, G. F. Chen, J. L. Luo, N. L. Wang, E. W. Carlson, J. Hu, and P. Dai, Phys. Rev. Lett. **101**, 167203 (2008).
- ¹² S.O. Diallo, V.P. Antropov, T.G. Perring, C. Broholm, J.J. Pulikkotil, N. Ni, S.L. Bud'ko, P.C. Canfield, A. Kreyssig, A.I. Goldman and R.J. McQueeney, Phys. Rev. Lett. **102**, 187206 (2009).
- ¹³ R. Applegate, J. Oitmaa, R. R. P. Singh, Phys. Rev. B **81**, 024505 (2010).
- ¹⁴ Jun Zhao, D. T. Adroja, Dao-Xin Yao, R. Bewley, Shiliang Li, X. F. Wang, G. Wu, X. H. Chen, Jiangping Hu, Pengcheng Dai, Nature Physics **5**, 555 (2009).
- ¹⁵ C. Lester, Jiun-Haw Chu, J. G. Analytis, T. G. Perring, I. R. Fisher, S.M. Hayden, Phys. Rev. B **81**, 064505 (2010).
- ¹⁶ Subir Sachdev, *Quantum Phase Transitions* (Cambridge University Press, Cambridge, 2001).
- ¹⁷ M. M. Qazilbash, J. J. Hamlin, R. E. Baumbach, Lijun Zhang, D. J. Singh, M. B. Maple, D. N. Basov, Nature Physics **5**, 647 (2009).
- ¹⁸ S. E. Sebastian, J. Gillett, N. Harrison, P. H. C. Lau, C. H. Mielke, G. G. Lonzarich, J. Phys.: Condens. Matter **20**, 422203 (2008).

- ¹⁹ James G. Analytis, Ross D. McDonald, Jiun-Haw Chu, Scott C. Riggs, Alimamy F. Bangura, Chris Kucharczyk, Michelle Johannes, I. R. Fisher, Phys. Rev. B **80**, 064507 (2009).
- ²⁰ P. Richard, K. Nakayama, T. Sato, M. Neupane, Y.-M. Xu, J. H. Bowen, G. F. Chen, J. L. Luo, N. L. Wang, X. Dai, Z. Fang, H. Ding, T. Takahashi, Phys. Rev. Lett. **104**, 137001 (2010).
- ²¹ X. F. Wang, T. Wu, G. Wu, H. Chen, Y. L. Xie, J. J. Ying, Y. J. Yan, R. H. Liu, and X. H. Chen, Phys. Rev. Lett. **102**, 117005 (2009).
- ²² Tao Li, J. Phys.: Condens. Matter **20**, 425203 (2008).
- ²³ P. W. Anderson, Phys. Rev. **86**, 694 (1952).
- ²⁴ C. Lanczos, J. Research National Bureau of Standards **45** (4), 255 (1950).
- ²⁵ R.B. Lehoucq, D.C. Sorensen and C. Yang, *ARPACK Users' Guide* (SIAM, Philadelphia, 1998).
- ²⁶ K. Haule and G. Kotliar, New J. Phys. **11**, 025021 (2009).
- ²⁷ W. L. Yang, A. P. Sorini, C-C. Chen, B. Moritz, W.-S. Lee, F. Vernay, P. Olalde-Velasco, J. D. Denlinger, B. Delley, J.-H. Chu, J. G. Analytis, I. R. Fisher, Z. A. Ren, J. Yang, W. Lu, Z. X. Zhao, J. van den Brink, Z. Hussain, Z.-X. Shen, T. P. Devereaux, Phys. Rev. B **80**, 014508 (2009).
- ²⁸ Takeshi Kondo, R. M. Fernandes, R. Khasanov, Chang Liu, A. D. Palczewski, Ni Ni, M. Shi, A. Bostwick, E. Rotenberg, J. Schmalian, S. L. Bud'ko, P. C. Canfield, A. Kaminski, Phys. Rev. B **81**, 060507(R) (2010).
- ²⁹ N. Harrison and S.E. Sebastian, Phys. Rev. B **80**, 224512 (2009).